Quantitative optical measurement of chemical potentials in intermediate band solar cells

Pierre Rale, Amaury Delamarre, Gilbert El-Hajje, Ryo Tamaki, Kentaroh Watanabe, Yasushi Shoji, Yoshitaka Okada, Masakazu Sugiyama, Laurent Lombez, Jean-François Guillemoles

Journal of Photonics for Energy

PhotonicsforEnergy.SPIEDigitalLibrary.org

Quantitative optical measurement of chemical potentials in intermediate band solar cells

Pierre Rale
Amaury Delamarre
Gilbert El-Hajje
Ryo Tamaki
Kentaroh Watanabe
Yasushi Shoji
Yoshitaka Okada
Masakazu Sugiyama
Laurent Lombez
Jean-François Guillemoles

SPIE.

Quantitative optical measurement of chemical potentials in intermediate band solar cells

Pierre Rale,[a] Amaury Delamarre,[a,b] Gilbert El-Hajje,[a] Ryo Tamaki,[b,c] Kentaroh Watanabe,[b,c] Yasushi Shoji,[c] Yoshitaka Okada,[b,c] Masakazu Sugiyama,[b,c] Laurent Lombez,[a] and Jean-François Guillemoles[a,b,*]

[a]CNRS, Institut de Recherche et Développement sur l'Energie Photovoltaïque, EDF R&D 6 quai Watier, Chatou 78401, France

[b]The University of Tokyo, NextPV, CNRS-RCAST Joint Lab, Tokyo, Meguro-ku 153-8904, Japan

[c]The University of Tokyo, Research Center for Advanced Science and Technology, Tokyo, Meguro-ku 153-8904, Japan

Abstract. Having shown some demonstration of two photon absorption and multiband emission processes in quantum dots (QD), multiquantum wells (MQW), and highly mismatched alloys, intermediate band solar cells are currently the subject of numerous studies. To better understand the underlying mechanisms, our objective is to experimentally probe the multiband operation of this device. We used photoluminescence recorded with a calibrated hyperspectral imager which provides spectrally resolved images with a spatial resolution of 2 μm and spectral resolution of 2 nm on proof of concept QD and MQW solar cells samples. Device emission can be described with the generalized Planck's law from which the quasi-Fermi level splitting of the three bands can be determined. The advantage of the technique is that it can be used to investigate the intermediate band material without the need to make contacts or a full device structure. We also discuss the usefulness of a dual-beam method. © *2015 Society of Photo-Optical Instrumentation Engineers (SPIE)* [DOI: 10.1117/1.JPE.5.053092]

Keywords: photovoltaics; intermediate band solar cells; characterization; photoluminescence; multiquantum wells; quantum dots.

Paper 14052SSP received Sep. 22, 2014; accepted for publication May 4, 2015; published online Jun. 5, 2015.

1 Introduction

Intermediate band solar cells (IBSC) or intermediate level solar cells, depending on whether the midgap states are localized or not, have been proposed[1–3] as a way to overcome the Shockley–Queisser limit[4] of solar cell efficiencies. An IBSC would be able to provide the same conversion efficiency as a triple junction, in principle, due to the three allowed interband optical transitions in the material (Fig. 1). All the generation paths also work, of course, as recombination pathways, but when optical cross sections of the transitions are larger than the nonradiative ones, and if the transition energies are well chosen, this configuration leads to a net efficiency gain as is well documented.[5,6] Systems proposed to be able to display IBSC photovoltaic conversion include III/V hetero-structures like multiquantum wells (MQW) and quantum dots (QD), where some partial evidences of such an effect has been found in the form of evidence for two photon absorption both in QW[7] and in QD solar cells,[8–10] and highly mismatched alloys.[11] As it turns out, these effects are relatively small (several orders of magnitude smaller than the direct band to band absorption), and can be mixed with other effects such as induced temperature variations, charging/discharging of trap states or even second harmonic generation. This makes it very difficult to nonambiguously characterize that a material or device is operating as an IBSC.

*Address all correspondence to: Jean-François Guillemoles, E-mail: jf.guillemoles@chimie-paristech.fr

1947-7988/2015/$25.00 © 2015 SPIE

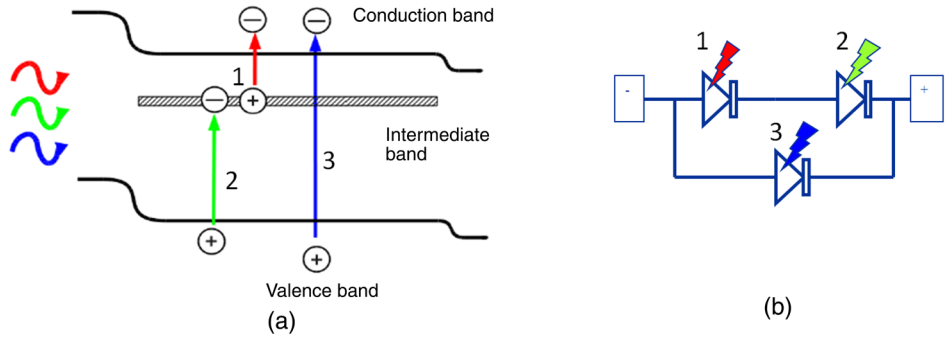

Fig. 1 (a) Band diagram of an intermediate band material and electrical equivalent circuit of an IBSC device illustrating the transitions in an intermediate band device. Additionally to the normal band to band transition (3), transitions (1) and (2) are also conducive to the promotion of an electron. All the generation paths indicated work also of course as recombination pathways. (b) Equivalent circuit of the IBSC with three diodes.

A long searched hallmark for IBSC operation is the identification of the three transitions where the quasi-Fermi level (QFL) separation of carriers corresponding to the high energy transition is the sum of the two others, as in, for example, Refs. 3 and 12:

$$\Delta\mu_1 + \Delta\mu_2 = \Delta\mu_3, \tag{1}$$

where $\Delta\mu$ denotes the QFL (that is the chemical potential of radiation in this case) and the indices refer to the transition (as in Fig. 1). Such a measurement can be performed by using photoluminescence (PL), and therefore, does not involve the completion of the device: the IBSC absorber alone can be characterized. This differs from approaches relying on electroluminescence to assess the QLF splitting in similar structures[13,14] and that have attracted criticism for application to QD solar cells.[15]

The present work associates state of the art quantum confined heterostructures with a calibrated hyperspectral imager able to map QFL splitting of transitions in the NIR-visible range. Using this unique tool, the QFL corresponding to the various transitions has been measured in several samples and is discussed. This work shows how, in principle, IBSC operation could be studied in materials even in the absence of a complete device. To show the proof of principle of the IBSC operation measurement, we use a MQW solar cell with three possible interband or intraband transitions.

2 Method Principle

To perform the analysis, we took advantage of the luminescence emission of the sample. This one can be described by the generalized Planck's law[16,17] for an infinitesimal volume element

$$\varphi(\hbar\omega) = \alpha(\hbar\omega)\frac{n^2}{4\pi^3\hbar^3c_0^2}(\hbar\omega)^2\frac{1}{\exp\left(\frac{\hbar\omega-\Delta\mu(\hbar\omega)}{kT}\right)-1}, \tag{2}$$

$\phi(\hbar\omega)$ is the luminescence emission per volume unit, ω is the photon energy, α is the absorption coefficient, Ω is the solid angle of emission, n is the optical index, $\hbar$ is the reduced Planck's constant, c_0 is the speed of light in vacuum, $\Delta\mu(\hbar\omega)$ is the local QFL splitting, and T is the temperature. Since the observed photon energy is sufficiently larger than the QFL splitting, we will use the Boltzmann approximation. To simplify the notation, we also introduce the black body emission flux

$$\varphi_{bb}(\hbar\omega) = \frac{1}{4\pi^3\hbar^3c_0^2}(\hbar\omega)^2\frac{1}{\exp\left(\frac{\hbar\omega}{kT}\right)-1}. \tag{3}$$

Experimentally, only the emission from the surface can be measured so that Eq. (2) must be integrated over the emitting volume. Considering the emission normal to the surface, in a sample of thickness d

$$\Phi(\hbar\omega) = \varphi_{bb}(\hbar\omega) \int_0^d \alpha(\hbar\omega, z) P(\hbar\omega, z) \exp\left[\frac{\Delta\mu(\hbar\omega, z)}{kT}\right] \mathrm{d}z, \tag{4}$$

$P(\hbar\omega, z)$ is the probability for a photon of energy $\hbar\omega$, emitted at a depth z, to be emitted from the surface, taking into account absorption, reflection, and eventual interferences. This probability is the same as the probability for a photon of energy $\hbar\omega$ incident on the surface to be absorbed at the depth z. The equation is simplified in case $\Delta\mu$ is constant throughout the sample, which is true in solar cells that exhibit sufficiently long diffusion lengths. We can write

$$\Phi(\hbar\omega) = A(\hbar\omega)\varphi_{bb}(\hbar\omega) \exp\left[\frac{\Delta\mu(\hbar\omega)}{kT}\right], \tag{5}$$

where $A(\hbar\omega)$ is the absorption probability of a photon of energy $\hbar\omega$ incident on the surface. Indeed, $A(\hbar\omega) = \int_0^d \alpha(\hbar\omega, z) P(\hbar\omega, z) \mathrm{d}z$. Eventually, the QFL splitting can be determined from the luminescence

$$\Delta\mu(\hbar\omega) = kT \ln\left[\frac{\Phi(\hbar\omega)}{A(\hbar\omega)\varphi_{bb}(\hbar\omega)}\right]. \tag{6}$$

We note here that with a relative measurement of the luminescence, the QFL splitting can only be determined with an unknown offset.

In some cases, especially in low performance devices, $\Delta\mu$ could be not uniform in the depth of the sample. For generality, we will consider the QFL splitting determined from luminescence as an effective splitting, noted $\Delta\mu_{eff}$. Nevertheless, even in the worst cases where the QFL splitting strongly fluctuates, $\Delta\mu_{eff}$ is close to the maximum value taken by $\Delta\mu(z)$. This is due to the exponential dependence of the luminescence on the QFL splitting, as will be discussed in Sec. 5 for our samples.

We also note that the absorption $A(\hbar\omega)$ is not the total absorption, but only the absorption in the regions where $\Delta\mu \neq 0$ eV, i.e., the active parts of the cell. This value does not contain parasitic absorptions (e.g.,in a window layer) and is experimentally difficult to access. However, in a high performance cell in which the collection probability is one in the active parts, $A(\hbar\omega) = \mathrm{EQE}(\hbar\omega)$ with EQE being the external quantum efficiency, which is much easier to measure. As we will see, this assumption is valid for the samples studied in this communication.

3 Experimental Setup and Samples

3.1 *Experimental setup*

In order to record the samples' luminescence emission, we used a hyperspectral imager developed by Photon, etc (Montreal, Quebec, Canada). Either a Nikon objective of 0.4 numerical aperture or an optical lens of 70 mm focal length is used to image the samples, and a silicon CCD camera from Tucsen is used to record the luminescence. The microscope objective was used to image the center part of the cell [Fig. 5(b)], whereas the lens allowed monitoring the full surface [Fig. 5(c)]. It is worthwhile to note that the system can be easily modified to investigate cells from the micrometer scale to the centimeter scale. Indeed, surfaces recorded here represent a hundred fold increase over the previous demonstration.[18] A Keithley 2635B is used for the electric measurements. This setup acquires spectrally resolved images with a spatial resolution of 2 μm and spectral resolution of 2 nm. A method for the absolute calibration of the setup was previously published,[18] so the signal will be measured in photons emitted per second, surface unit, and energy interval. In the photoluminescence experiment, the excitation is performed with a 532 nm CW laser from Coherent. When the sample is contacted (as here), electroluminescence

can be used as long as series resistance effects are negligible. The whole setup is described in Fig. 2.

Hyperspectral imaging combines both the spatial and spectral dimensions of the luminescence. With various kind of photovoltaic technologies, such acquisitions were reported using either a scanning confocal microscope and a spectrometer,[19] or a line-scanning hyperspectral imager.[20–22] Nevertheless, none of these methods allowed an absolute calibration of the luminescence as reported here, which is necessary to determine the QFL splitting in absolute values.

From the above described setup, the luminescence can be obtained in the 400 to 1100 nm range, which allows us to study transitions from the valence band to conduction band, both in the QW and in GaAs layers. Intraband transitions cannot be studied.

3.2 *Samples*

In the present study, for proof of principle purposes, we have mainly used an MQW strain-balanced test device prepared by MOCVD, in epitaxy on GaAs, and comprising 20 wells in a pin structure, as described in Fig. 3. This sample is well studied[23] and performs as a standard MQW solar cell as shown in Fig. 4.

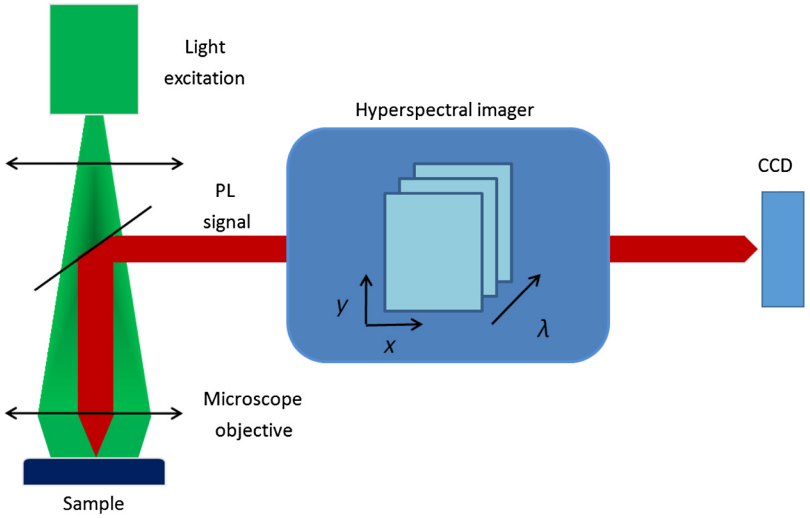

Fig. 2 Principle of hyperspectral imaging: experimental configuration for uniform sample excitation, a hyperspectral imager, and a CCD detection. A hypercube of data (x, y, λ, intensity) is acquired with a CCD camera as explained in the text. At each spatial location, a luminescence spectrum with calibrated data is obtained. Conversely, maps of luminescence intensities for each wavelength can be extracted.

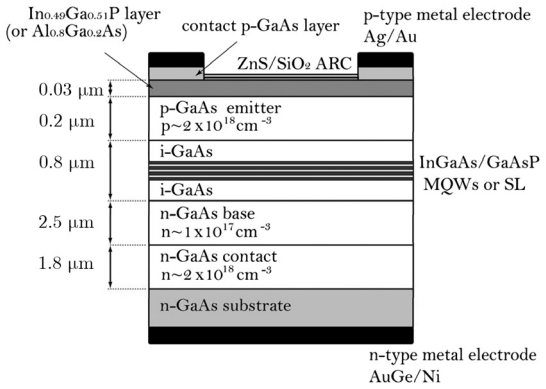

Fig. 3 Description of the multiquantum wells (MQW) sample. The composition well/barrier is $In_{0.2}Ga_{0.8}As/GaAs_{0.8}P_{0.2}$ for the 20 periods' well/barrier with respective thicknesses 8/12 nm.

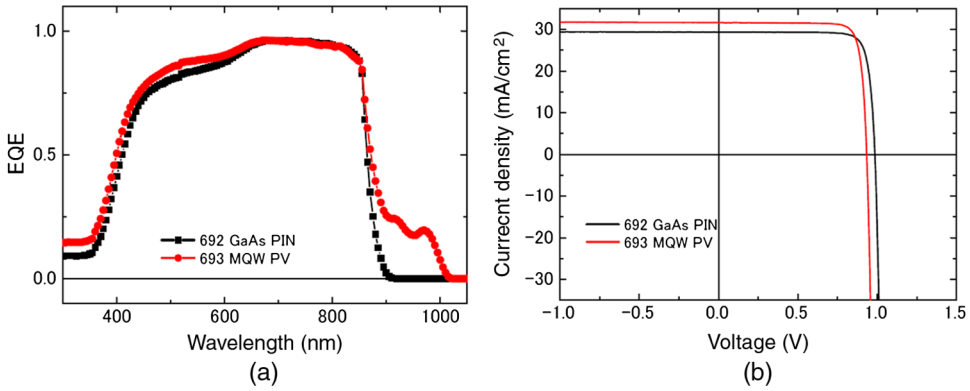

Fig. 4 External quantum efficiency of the MQW sample, compared to a reference GaAs pin solar cell of the same structure, but without the (a) QW and the (b) corresponding J-V curves.

Preliminary experiments have been also carried out on InAs QD solar cells samples embedded in an $Al_{0.2}Ga_{0.8}As$ matrix, similar to those described in Ref. 9, with 10 periods of QD. These samples have recently shown two photon absorption features.[9] In contrast, the absorptivity of the QD layers is difficult to measure or model, and the transport of charge is quite complex, which makes the validity of Eq. (6) questionable in this case.

4 Results

First, the MQW cell was illuminated either locally (1% of the total area in its center) or on its whole surface, and its luminescence signal has been collected by the hyperspectral imager. In Fig. 5 are shown the PL emission at 986 nm. We obtained open-circuit voltages and short-circuit current densities of 1.017 V and 280 mA/cm^2 for the local excitation, and 0.970 V and 170 mA/cm^2 for the global excitation. The illumination intensity was uniform at $\pm 10\%$ over the illuminated area in each case. The grid of the cell is clearly visible as it is shadowing the luminescence emitted from the inside of the device.

When the cell is fully and uniformly illuminated, the PL emission is also very uniform as is expected from such a sample. In contrast, partial illumination results in a nonuniform PL signal, decaying toward the grid and the edges of the image. The reason for this will be discussed below, but one can already understand the importance of a uniform illumination over the full sample for the acquisition of useful calibrated data.

The hyperspectral setup could also be used to test the uniformity of the sample. Under complete illumination, PL intensities were found to be very uniform, except for those at the absorption edge close to the PL emission peak, in which a gradient in peak maximum was found across the sample (6 meV over the 4.2 mm diagonal, Fig. 6), indicative of a slight shift of MQW thickness or/and composition, although this is of no consequence here.

The transformation given by Eq. (6) is illustrated in Fig. 7, where only the central 1% of the cell is illuminated to allow for a higher flux and, therefore, a better signal to noise ratio of the measurement (meaning a larger energy range can be accessed). The photons can be sorted in two ranges, those clearly originating from the wells (between 900 and 980 nm) and those with an energy above that of the GaAs bandgap (<870 nm) that may correspond to transitions either in the well material or in GaAs. Below and above the transition, for several excitation intensities, the QFL splitting determined experimentally (Fig. 7) is found to be pretty constant, with a variation of only about 10 meV. We note some bumps that are experimental artifacts because the EQE and the PL were not acquired with the same spectral resolution (10 and 2 nm, respectively). Therefore, the excitonic features and other variations of the absorptivity where the bumps are found are not taken into account.

Finally, another type of investigation could be attempted using the same setup by providing a double beam excitation. This is similar to previous experiments,[7,9–12] where two photon absorption was probed by EQE measurements under an additional IR irradiation bias to assess whether the carriers generated in the wells could be collected thanks to the absorption of low energy

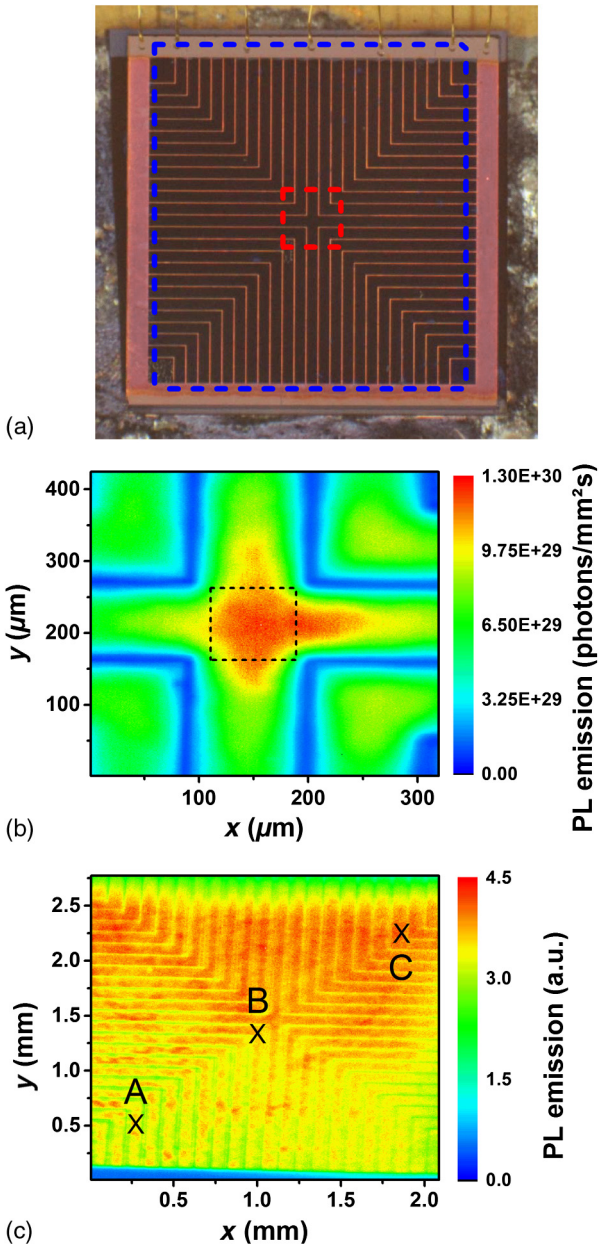

Fig. 5 (a) Optical image of the MQW solar cell. The device size is 3×3 mm^2. The dashed squares represent the imaged area for (red) local and (blue) global illumination. (b) and (c) Displayed the photoluminescence (PL) emission at 986 nm for respectively the local and global excitation. The boxed area in (b) corresponds to the area of averaging for the spectrum displayed in Fig. 7. In points A, B and, C in (c) are extracted the spectra displayed in Fig. 6(a).

photons by an intraband transition. In our experiment, we aim at finding the signature of two photon absorption in the PL signal rather than in the electric current.

A low power additional IR laser (1.5 μm) was accordingly pointed at the sample. The PL has been repeatedly measured with and without this additional excitation source to ensure the reliability of the data. In this case, it has not been possible to provide a uniform illumination of the full sample by both lasers as in the previous experiments, so that only a part of the device was seeing the IR illumination. Here, a full calibration of the measurements was not attempted and the PL data are displayed in arbitrary units. The results are presented in Fig. 8(a). It is seen that the IR illuminated sample sees a slightly reduced PL emission in the well region as compared to the GaAs region.

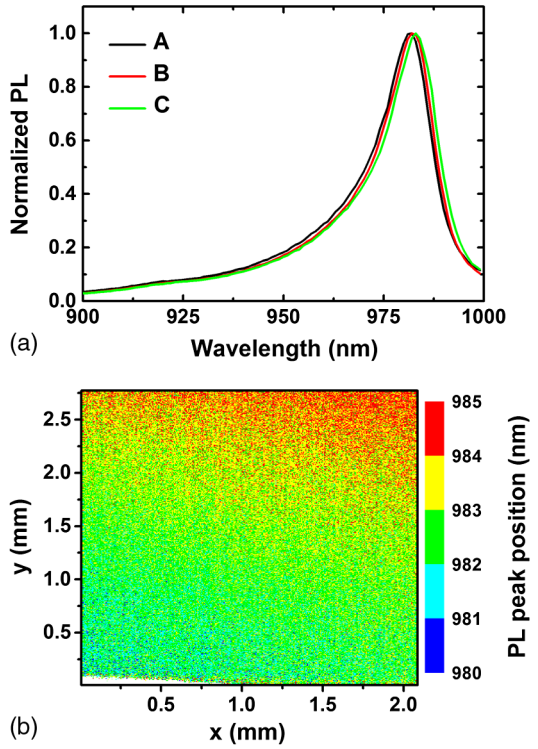

Fig. 6 (a) Spectra extracted at points A, B, and C (see Fig. 5) for the global illumination, on which we observe a drift of the PL maximum position. Plotting the PL peak position for each spatial point (b) shows a small gradient of 5 nm of the well depth across the cell.

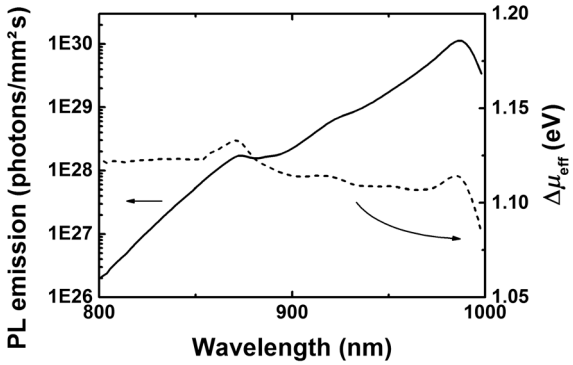

Fig. 7 PL spectrum (solid line) in logarithmic scale averaged on the red square [see Fig. 5(b)] and values of the quasi-Fermi level separation (dashed line) deduced from the application of the generalized Planck law.

Preliminary experiments have been also carried out on QD solar cells samples similar to those described in Ref. 9. We present here only the double beam experiment on the QD device on Fig. 8(b): this sample also shows an influence on the lower energy transitions of the IR additional source in the spectral region corresponding to the wetting layer (780 to 820 nm), but curiously, not in the spectral region corresponding the QD (>820 nm). In the high band gap material spectral region, a slight decrease of the PL is also observed.

5 Discussion

As for the interpretation of the determined QFL spectra, it is important to discuss the validity and the consequences of the hypothesis made in Sec. 2. The assumptions were that (1) $A = \text{EQE}$ and (2) $\Delta\mu$ is constant throughout the sample depth.

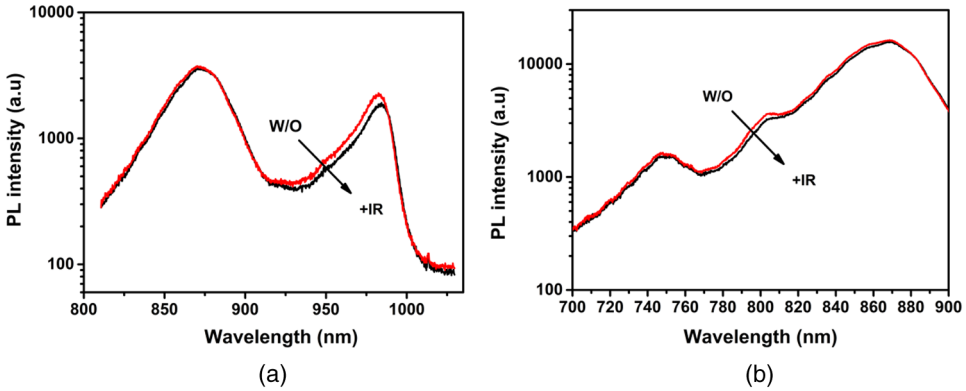

Fig. 8 PL (a) of the MQW solar cell and (b) of the QD solar cell with and without additional IR excitations.

With respect to (1), the EQE presented in Fig. 4 takes values around 0.2 in the wavelength range of the QW absorption. Since the cell contains only 20 QW, this is a rather large value, implying that the collection is close to unity. Nevertheless, because the absorption necessarily takes values between the EQE and 1, the maximum error would be a factor of 5. Due to the exponential dependence of the luminescence on the QFL splitting, this factor of 5 results in a maximum error of about 40 meV on $\Delta\mu$, i.e., between 3 and 4% of the determined $\Delta\mu_{\text{eff}}$ in our case, depending on the excitation intensity.

With respect to (2), in real devices, the QFL sliptting is not uniform within the device and can vary, especially with depth.[24] Moreover we should make the difference between the emission above the GaAs bandgap, which can be emitted at any position in the device, and the emission at lower energies, which must originate from the QW. Let us first consider the QW emission. We should again take into account that the cell contains only 20 wells. This is a favorable case for error estimation, since one can estimate the most inhomogeneous $\Delta\mu(z)$ profile possible, which would be that it takes a value different from 0 eV in only one well. In that extreme case, the difference between $\Delta\mu_{\text{eff}}$ and the $\Delta\mu(z)$ maxima would be only 80 meV, i.e., around 7% of the determined values. This illustrates that $\Delta\mu_{\text{eff}}$ mainly reflects the maximum of the QFL splitting. Nevertheless this extreme depth profile is highly improbable since the EQE from the QW was shown to be large, reflecting efficient carrier transport in the QW region, which implies uniform QFL splitting. Considering the emission above the GaAs bandgap, the EQE is close to unity in that wavelength range, which implies good carrier transport properties in the absorption region of those photons. Since the good transport properties imply uniform carrier distribution and the absorption and emission region are the same, assumption (2) holds in that wavelength range.

To summarize, we can state that, in our samples, $\Delta\mu$ cannot have a strong depth dependence and the EQE is a good approximation of the absorption. This is due to efficient carrier transport. As a consequence, the experimentally monitored $\Delta\mu_{\text{eff}}$ reflects the value taken by $\Delta\mu$ with high precision. Moreover, we have seen that, even in much less favorable cases where assumptions (1) and (2) are not strictly true, $\Delta\mu_{\text{eff}}$ is a good approximation of the $\Delta\mu$ maximum. Those reasons explain why, experimentally, a good agreement is found between $\Delta\mu_{\text{eff}}$ measured by this technique and V_{oc}.[18,24,25]

As for the samples investigated in this paper, we can now draw conclusions from the QFL splitting spectra in Fig. 7. It appears that $\Delta\mu_{\text{eff}}$ takes similar values above and below the GaAs bandgap. This means that the QFL splitting corresponding to the carrier population in the confined state is the same as that for everywhere else in the sample. Therefore, this sample, in these operating conditions at least, does not work as an IBSC device.

As is clear from the importance of the grid pattern and edges, the nonuniformity in the images taken over a partially illuminated cell is due to lateral transport toward the nonilluminated part of the cell. Indeed, a gradient in QFL of the carriers has to result in carrier transport. This gradient results from the creation of a large number of electron-hole pairs in the illuminated area while none is created in the nonilluminated area. In the presence of highly conducting layers in a pin structure, pairs are collected at the contacts before they recombine. The conducting layers, and

especially the grid, tend to restore the equipotential character of the contacts that the nonuniform photocarrier generation has been disrupting. The final distribution is the result of the competition between local generation and transport.

For the localized excitation, after integration on the photon energies, we found QFL splitting values ranging from 1.11 eV (close to the contacts) to 1.13 eV (at the image center). To the best of the authors' knowledge, this is the first time that an absolute determination of the QFL splitting with spatial resolution is demonstrated on a sample used for IBSC proof of concept.

Finally, as is well known, intermediate band materials will not enable an efficiency gain unless the optical processes are faster than the nonradiative ones.[5,6] Indeed, intermediate bands or levels would induce losses through additional carrier recombination as well as gains from additional generation. The balance is clearly associated with the strength of the optical transitions between levels. If the optical transitions' oscillator strength is large enough, optical pumping between levels results in a QFL splitting, that is, the conversion of radiative energy into electrochemical free energy that can then be collected as electrical work.[17] It is the purpose of the double beam experiments that have been carried out to probe the optical rates. This experimental approach is interesting in that it enables us to probe the system optically only without the need for electrical contacts or to complete the device. The investigation can be done at the material level only.

In both of our samples, these experiments consistently showed a distinct and repeatable influence of the IR probe beam on the PL. In the framework of an IBSC operation, the IR beam, pumping electrons from the well states into the conduction band, should ideally manifest itself by a reduction of the PL signal from the wells (because the carrier density is slightly reduced), which is observed experimentally, and by a simultaneous increase of the PL from the conduction band states (because the carrier density of these states is slightly increased), which is not observed. It may be that the IR probe, however weak, is inducing some heating of the sample which reduces the PL yield. Moreover, the QD do not appear, in contrast to wells (in the MQW sample and in the wetting layers), to show a reduced PL under IR bias. This is probably indicative of their weak optical cross section.

6 Conclusion and Perspectives

In summary, the originality of the work lies in the utilization of a unique method developed in one of the participating institutes to directly measure a key property of solar cells: their QFL splitting under illumination. Based on this measurement setup, we have proposed a method and shown that assessing materials for their suitability for an application in IBSC devices could be done without having to actually make and optimize the full device. This is an important advantage for a relatively immature technology such as IBSC devices. The samples used for the proof of principle were not found to exhibit the required QFL splitting for IBSC operation.

Finally, we have also proposed a double beam experiment to optically probe the optical rates for inter or intraband transition. Our samples exhibited a weak, but measurable, influence on the PL signal from the IR probe. This influence cannot be completely explained as yet. As a possible perspective, this double beam experiment could, in principle, be calibrated, yielding quantitative data on the optical transition rates between the bands.

Acknowledgments

JFG acknowledges the support of JSPS in the form of a short term fellowship during the summer 2013.

References

1. M. Wolf, "Limitations and possibilities for improvement of photovoltaic solar energy converters: part I: considerations for earth's surface operation," *Proc. IRE* **48**(7), 1246–1263 (1960).
2. J.-F. Guillemoles and S. Kettemann, "Limiting efficiencies of LDS intermediate band solar cells," in *13th European Photovoltaic Solar Energy Conference*, p. 119 (1995).
3. A. Luque and A. Martí, "Increasing the efficiency of ideal solar cells by photon induced transitions at intermediate levels," *Phys. Rev. Lett.* **78**(26), 5014–5017 (1997).

4. W. Shockley and H. J. Queisser, "Detailed balance limit of efficiency of p-n junction solar cells," *J. Appl. Phys.* **32**(3), 510 (1961).
5. P. Olsson, C. Domain, and J.-F. Guillemoles, "Ferromagnetic compounds for high efficiency photovoltaic conversion: the case of AlP:Cr," *Phys. Rev. Lett.* **102**(22), 227204 (2009).
6. J. Yuan et al., "Positive or negative gain: role of thermal capture cross sections in impurity photovoltaic effect," *J. Appl. Phys.* **110**(10), 104508 (2011).
7. M. Sugiyama et al., "Photocurrent generation by two-step photon absorption with quantum-well superlattice cell," *IEEE J. Photovoltaics* **2**(3), 298–302 (2012).
8. A. Martí et al., "Production of photocurrent due to intermediate-to-conduction-band transitions: a demonstration of a key operating principle of the intermediate-band solar cell," *Phys. Rev. Lett.* **97**(24), 247701 (2006).
9. Y. Shoji, K. Akimoto, and Y. Okada, "Optical properties of multi-stacked InGaAs/GaNAs quantum dot solar cell fabricated on GaAs (311)B substrate," *J. Appl. Phys.* **112**(6), 064314 (2012).
10. I. Ramiro et al., "Review of experimental results related to the operation of intermediate band solar cells," *IEEE J. Photovoltaics* **4**(2), 736–748 (2014).
11. N. López et al., "Engineering the electronic band structure for multiband solar cells," *Phys. Rev. Lett.* **106**(2), 028701 (2011).
12. A. Luque et al., "Understanding the operation of quantum dot intermediate band solar cells," *J. Appl. Phys.* **111**(4), 044502 (2012).
13. E. Tsui et al., "Determination of the quasi-Fermi-level separation in single-quantum-well p-i-n diodes," *J. Appl. Phys.* **80**(8), 4599 (1996).
14. N. López et al., "Experimental analysis of the operation of quantum dot intermediate band solar cells," *J. Sol. Energy Eng.* **129**(3), 319–322 (2007).
15. A. A. Abouelsaood, M. Y. Ghannam, and J. Poortmans, "On the reported experimental evidence for the quasi-Fermi level split in quantum-dot intermediate-band solar cells: Quasi-Fermi level split in quantum-dot IBSCs," *Prog. Photovoltaics Res. Appl.* **21**(2), 209–216 (2013).
16. B. Feuerbacher and P. Wurfel, "Verification of a generalised Planck law by investigation of the emission from GaAs luminescent diodes," *J. Phys. Condens. Matter* **2**(16), 3803–3810 (1990).
17. P. Würfel, Ed., *Physics of Solar Cells: From Basic Principles to Advanced Concepts*, 2nd ed., Wiley-VCH, Weinheim (2009).
18. A. Delamarre, L. Lombez, and J.-F. Guillemoles, "Contactless mapping of saturation currents of solar cells by photoluminescence," *Appl. Phys. Lett.* **100**(13), 131108 (2012).
19. L. Gütay and G. H. Bauer, "Spectrally resolved photoluminescence studies on Cu(In,Ga) Se2 solar cells with lateral submicron resolution," *Thin Solid Films* **515**(15), 6212–6216 (2007).
20. M. P. Peloso et al., "Evaluating the electrical properties of silicon wafer solar cells using hyperspectral imaging of luminescence," *Appl. Phys. Lett.* **99**(22), 221915 (2011).
21. E. Olsen and A. S. Flø, "Spectral and spatially resolved imaging of photoluminescence in multicrystalline silicon wafers," *Appl. Phys. Lett.* **99**(1), 011903 (2011).
22. Q. Li et al., "Detection of physical defects in solar cells by hyperspectral imaging technology," *Opt. Laser Technol.* **42**(6), 1010–1013 (2010).
23. H. Fujii et al., "Suppressed lattice relaxation during InGaAs/GaAsP MQW growth with InGaAs and GaAs ultra-thin interlayers," *J. Cryst. Growth* **352**(1), 239–244 (2012).
24. A. Delamarre et al., "Quantitative luminescence mapping of $Cu(In,Ga)Se_2$ thin-film solar cells: quantitative luminescence mapping of CIGS thin-film solar cells," *Prog. Photovoltaics Res. Appl.* (2014).
25. A. Delamarre et al., "Evaluation of micrometer scale lateral fluctuations of transport properties in CIGS solar cells," *Proc. SPIE* **8620**, 862009 (2013).

Biographies of the authors are not available.